Stanislav Sysala
Estimation of EDZ zones in great depths by elastic-plastic models

In: Jan Chleboun and Pavel Kůs and Jan Papež and Miroslav Rozložník and Karel Segeth and Jakub Šístek (eds.): Programs and Algorithms of Numerical Mathematics, Proceedings of Seminar. Jablonec nad Nisou, June 19-24, 2022. Institute of Mathematics CAS, Prague, 2023. pp. 229–238.

Persistent URL: http://dml.cz/dmlcz/703203

Programs and Algorithms of Numerical Mathematics 21
J. Chleboun, P. Kůs, J. Papež, M. Rozložník, K. Segeth, J. Šístek (Eds.)
Institute of Mathematics CAS, Prague 2023

ESTIMATION OF EDZ ZONES IN GREAT DEPTHS BY ELASTIC-PLASTIC MODELS

Stanislav Sysala

Institute of Geonics of the Czech Academy of Sciences
Studentská 1768, 708 00 Ostrava, Czech Republic
stanislav.sysala@ugn.cas.cz

Abstract: This contribution is devoted to modeling damage zones caused by the excavation of tunnels and boreholes (EDZ zones) in connection with the issue of deep storage of spent nuclear fuel in crystalline rocks. In particular, elastic-plastic models with Mohr-Coulomb or Hoek-Brown yield criteria are considered. Selected details of the numerical solution to the corresponding problems are mentioned. Possibilities of elastic and elastic-plastic approaches are illustrated by a numerical example.

Keywords: tunnel stability, EDZ zones, elasto-plasticity, finite element method

MSC: 74C05, 65N30

1. Introduction

Zones with higher stress concentrations, formation and joining of cracks of various sizes or with V-shaped notches can be observed on tunnel walls and in their vicinity as a consequence of excavation and other effects. Such zones are usually called as excavation damage zones (EDZ). Prediction of EDZ is important for safety assessment in many applications. Our particular motivation is related to deep storage of spent nuclear fuel in crystalline rocks where EDZ can simplify transport of radionuclides. In order to predict EDZ and analyze coupled processes in these zones, various in-situ experiments have been carried out in underground research laboratories around the world. For example, we mention the Äspö pillar stability experiment carried out in Sweden [1] or the Tunnel Sealing Experiment (TSX) in Canada [8].

The most important factor that causes the formation of EDZ is the initial stress state in the rock mass. EDZ may depend on its magnitude, the ratios between the principal stresses and on the orientation of the principal stress directions with respect to the tunnel. EDZ also depends on the shape of the tunnel and its dimensions, the method of excavation, mechanical properties of the rock mass or its geological structure. EDZ can also expand after the excavation due to surrounding sites or

DOI: 10.21136/panm.2022.21

thermal heating [1]. On the contrary, bentonite barriers of a deep repository [1] can contribute to the stabilization of EDZ zones.

Mathematical modeling of EDZ can be based on continuum mechanics, fracture mechanics or on multiscale approaches. In this contribution, we focus on the continuum models, namely on elastic and elastic-plastic models. The elastic models are usually combined with a failure criterion to detect zones with high stress concentrations. Such a treatment is the simplest one and is convenient for large-scale 3D geometries. Next, one can consider elastic-plastic models where the failure criterion is directly a part of the model and admissible stress fields must satisfy the criterion. These models can be enriched with internal variables representing softening/hardening variable or damage variable. In the article [7] and related papers, different types of damage zones were classified based on elastic-plastic models, the so-called DISL approach.

This contribution consists of the following parts. Section 2 contains selected details to an abstract elastic-perfectly plastic problem and its solution scheme. Section 3 is devoted to the Mohr-Coulomb and Hoek-Brown constitutive models and their solution. Section 4 contains a numerical example illustrating possibilities of elastic and elastic-plastic approaches of modeling EDZ zones. Concluding remarks can be found in Section 5.

2. Numerical scheme of the elastic-perfectly plastic model

We consider a simplified 2D geometry of the rock mass around the tunnel depicted in Figure 1. The square domain and its subdomain without the tunnel will be denoted as $\widehat{\Omega}$ and Ω, respectively. We prescribe zero normal displacements on the outer boundary $\partial\widehat{\Omega}$ (far the from tunnel) and zero normal stress on the inner boundary Γ, that is, $\boldsymbol{u}\cdot\boldsymbol{n} = 0$ on $\partial\widehat{\Omega}$ and $\boldsymbol{\sigma}\boldsymbol{n} = \boldsymbol{0}$ on Γ, where $\boldsymbol{u}$, $\boldsymbol{\sigma}$, and $\boldsymbol{n}$ denote the displacement field, the Cauchy stress field, and the outward unit normal vector to Ω, respectively. We prescribe the initial stress field $\boldsymbol{\sigma}_0$ defined in Ω. For the sake of simplicity, we simulate the tunnel excavation by the load history $t\boldsymbol{\sigma}_0/t_{\max}$, where $t \in [0, t_{\max}]$. Next ingredients of the elastic and elastic-plastic models are the infinitesimally small

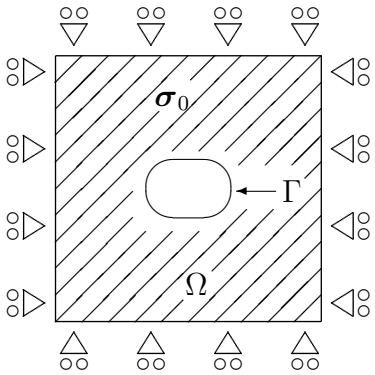

Figure 1: 2D geometry of the rock mass around the tunnel.

strain tensor

$$\boldsymbol{\varepsilon} := \boldsymbol{\varepsilon}(\boldsymbol{u}) = \frac{1}{2}(\nabla \boldsymbol{u} + (\nabla \boldsymbol{u})^T)$$

and the fourth-order elastic tensor $\mathbb{C}$,

$$\begin{aligned} \mathbb{C}\boldsymbol{\varepsilon} &= \frac{E}{1+\nu}\left\{\frac{\nu}{1-2\nu}(\text{tr } \boldsymbol{\varepsilon})\boldsymbol{I} + \boldsymbol{\varepsilon}\right\}, \\ \mathbb{C}^{-1}\boldsymbol{\sigma} &= -\frac{\nu}{E}(\text{tr } \boldsymbol{\sigma})\boldsymbol{I} + \frac{1+\nu}{E}\boldsymbol{\sigma}, \end{aligned}$$

where $E > 0$, $\nu \in (0, 1/2)$ denote Young's modulus and Poisson's ratio, respectively, $\boldsymbol{I}$ is the unit second-order tensor and $\text{tr } \boldsymbol{\varepsilon} = \boldsymbol{\varepsilon} : \boldsymbol{I} = \varepsilon_{11} + \varepsilon_{22} + \varepsilon_{33}$ is the trace of $\boldsymbol{\varepsilon}$.

In case of linear elasticity, we have the following constitutive (Hook's) law between the stress and strain tensors:

$$\boldsymbol{\sigma} = \mathbb{C}\boldsymbol{\varepsilon} + \boldsymbol{\sigma}_0 \quad \text{or} \quad \boldsymbol{\sigma} = \mathbb{C}[\boldsymbol{\varepsilon} + \boldsymbol{\varepsilon}_0], \;\; \boldsymbol{\varepsilon}_0 = \mathbb{C}^{-1}\boldsymbol{\sigma}_0.$$

Now, we introduce the elastic-perfectly plastic constitutive model, which is time-dependent. Let $\boldsymbol{\varepsilon}^e$ and $\boldsymbol{\varepsilon}^p$ denote the elastic and plastic parts of the strain tensor and λ is the plastic multiplier. We also define yield function $f := f(\boldsymbol{\sigma})$ and plastic potential $g := g(\boldsymbol{\sigma})$ and assume that these functions are convex. Then the corresponding evolution problem reads: for any $t \in (0, t_{\max})$, find $\boldsymbol{\sigma} := \boldsymbol{\sigma}(t)$, $\boldsymbol{\varepsilon} := \boldsymbol{\varepsilon}(t)$, $\boldsymbol{\varepsilon}^e := \boldsymbol{\varepsilon}^e(t)$, $\boldsymbol{\varepsilon}^p := \boldsymbol{\varepsilon}^p(t)$, $\lambda := \lambda(t)$ such that

- $\boldsymbol{\varepsilon} = \boldsymbol{\varepsilon}^e + \boldsymbol{\varepsilon}^p$, $\boldsymbol{\sigma} = \mathbb{C}(\boldsymbol{\varepsilon}^e + t\boldsymbol{\varepsilon}_0/t_{\max})$,
- $\dot{\boldsymbol{\varepsilon}}^p \in \dot{\lambda}\partial g(\boldsymbol{\sigma})$, $\boldsymbol{\varepsilon}^p(0) = 0$,
- $\dot{\lambda} \geq 0$, $\dot{\lambda} f(\boldsymbol{\sigma}) = 0$, $f(\boldsymbol{\sigma}) \leq 0$.

Here, the dot symbol means the time derivative and $\partial g(\boldsymbol{\sigma})$ denotes the subdifferential of g at $\boldsymbol{\sigma}$. It is worth-noticing that subdifferentials are not so obvious in engineering practice and the plastic flow rule is usually written by the derivative of g:

$$\dot{\boldsymbol{\varepsilon}}^p = \dot{\lambda}\frac{\partial g(\boldsymbol{\sigma})}{\partial \boldsymbol{\sigma}},$$

despite the fact that g is often non-differentiable. One of the aim of our work is to show that the knowledge of an explicit form of the set $\partial g(\boldsymbol{\sigma})$ can simplify analysis and constitutive solution for various elastic-plastic models. This was shown in [9, 10].

The elastic-plastic constitutive problem is mostly discretized by the implicit Euler method. Consider the partition $0 = t_0 < t_1 < \ldots < t_{k-1} < t_k < \ldots < t_{\max}$ of the time interval. Then the discretized constitutive problem at the k-th step, $k = 1, 2, \ldots$, has the following scheme: given $\boldsymbol{\varepsilon}_0$, $\boldsymbol{\varepsilon}_k$, and $\boldsymbol{\varepsilon}^p_{k-1}$, find $\boldsymbol{\sigma}_k$ and $\boldsymbol{\varepsilon}^p_k$ such that

$$\boldsymbol{\sigma}_k = \boldsymbol{T}(\boldsymbol{\varepsilon}_k - \boldsymbol{\varepsilon}^p_{k-1} + t_k\boldsymbol{\varepsilon}_0/t_{\max}), \quad \boldsymbol{\varepsilon}^p_k = \boldsymbol{\varepsilon}_k + t_k\boldsymbol{\varepsilon}_0/t_{\max} - \mathbb{C}^{-1}\boldsymbol{\sigma}_k.$$

Here, the tensor-valued function $\boldsymbol{T}$ needs to be constructed. In general, one can find $\boldsymbol{T}$ only in an implicit form and construct it by an iterative procedure. This construction is based on the elastic prediction – plastic correction algorithm [4, 3, 9, 10]. Within the elastic prediction, we test whether the trial stress $\boldsymbol{\sigma}_k^{tr} = \mathbb{C}(\boldsymbol{\varepsilon}_k - \boldsymbol{\varepsilon}_{k-1}^p + t_k\boldsymbol{\varepsilon}_0/t_{\max})$ satisfies the failure criterion $f(\boldsymbol{\sigma}_k^{tr}) \leq 0$. If it is so then $\boldsymbol{\sigma}_k = \boldsymbol{\sigma}_k^{tr}$ and $\boldsymbol{\varepsilon}_k^p = \boldsymbol{\varepsilon}_{k-1}^p$. Otherwise, the plastic correction is applied to be the constraint $f(\boldsymbol{\sigma}_k) = 0$ satisfied. So we need to return the predicted stress to the failure surface and construct the so-called return mapping. Such a mapping can be interpreted as a generalized projection onto a convex set. It is also worth noticing that the function $\boldsymbol{T}$ is non-differentiable, but its semismoothness is expected and can be proven just by the subdifferential-based treatment [9, 10].

Using the function $\boldsymbol{T}$, the overall elastic-plastic problem in terms of displacements reads:

$$\text{find } \boldsymbol{u}_k \in V: \quad \int_\Omega \boldsymbol{T}(\varepsilon(\boldsymbol{u}_k) - \boldsymbol{\varepsilon}_{k-1}^p + t_k\boldsymbol{\varepsilon}_0/t_{\max}) : \boldsymbol{\varepsilon}(\boldsymbol{v})\,\mathrm{d}x = 0 \quad \forall \boldsymbol{v} \in V,$$

where

$$V = \{\boldsymbol{v} \in H^1(\Omega;\mathbb{R}^d) \mid \boldsymbol{v}\cdot\boldsymbol{n} = 0 \text{ on } \partial\widehat{\Omega}\}$$

is a space of admissible displacement fields. After a space discretization, we arrive at a system of non-linear equations. Such a system is usually solved by a non-smooth version of the Newton method. It requires to construct a generalized derivative of $\boldsymbol{T}$. Its construction for specific models will be briefly discussed in the next section.

3. The Mohr-Coulomb and Hoek-Brown constitutive models

The Mohr-Coulomb and Hoek-Brown constitutive models are usual in geotechnics. The functions f and g for these models are defined in terms of principal stresses. Therefore, we need to introduce the spectral decomposition of the Cauchy stress tensor:

$$\boldsymbol{\sigma} = \sum_{i=1}^{3} \sigma_i \mathbf{e}_i \otimes \mathbf{e}_i, \quad \sigma_1 \geq \sigma_2 \geq \sigma_3.$$

Here, $\sigma_i \in \mathbb{R}$, $\mathbf{e}_i \in \mathbb{R}^3$, $i = 1, 2, 3$, denote the eigenvalues (principle stresses), and the eigenvectors of $\boldsymbol{\sigma}$, respectively. We assume the ordering $\sigma_1 \geq \sigma_2 \geq \sigma_3$ of the eigenvalues of $\boldsymbol{\sigma}$. From now on, we shall work with a mechanical sign convention assuming positive values for a tension. (In geomechanics, opposite sign convention is usual.)

The Mohr-Coulomb model is defined by the functions

$$\begin{aligned} f(\boldsymbol{\sigma}) &= (1+\sin\phi)\sigma_1 - (1-\sin\phi)\sigma_3 - 2c\cos\phi, \\ g(\boldsymbol{\sigma}) &= (1+\sin\psi)\sigma_1 - (1-\sin\psi)\sigma_3, \end{aligned}$$

where $c > 0$, $\phi \in (0, \pi/2)$ and $\psi \in (0, \pi/2)$ are given material parameters denoting the cohesion, the friction angle and the dilatancy angle. It is expected that $\psi \leq \phi$.

The Hoek-Brown model is defined by the functions

$$\begin{aligned} f(\boldsymbol{\sigma}) &= \sigma_1 - \sigma_{ci}\Big(s - m_b\frac{\sigma_1}{\sigma_{ci}}\Big)^a - \sigma_3, \\ g(\boldsymbol{\sigma}) &= \sigma_1 - \sigma_{ci}\Big(s_g - m_g\frac{\sigma_1}{\sigma_{ci}}\Big)^{a_g} - \sigma_3, \end{aligned}$$

where $\sigma_{ci}, s, s_g, m_b, m_g > 0$ and $a, a_g \in (0,1)$ are given material parameters. More details to these parameters can be found in [3, 5, 6]. Briefly speaking, they are defined by empirical formulas containing usual material parameters for intact rock samples and two indices, the geological strength index GSI and the disturbance index D. GSI represents a structure of the surrounding rock mass and D characterizes a way of the excavation. To be the model well-defined, we assume that $s_g/m_g \geq s/m$, although we have not found such an assumption in literature. In the limit case $a = a_g = 1$, one can transform the Hoek-Brown model to the Mohr-Coulomb models one.

Admissible stress fields satisfy the condition $f(\boldsymbol{\sigma}) \leq 0$. For both the models, the corresponding set is convex and aligned with the hydrostatic axis (where $\sigma_1 = \sigma_2 = \sigma_3$). The Mohr-Coulomb set is a hexahedral pyramid in the space of the principle stresses with the apex at $\sigma_t = c/\tan\phi$. For the Hoek-Brown model, the pyramid is curved and has the apex at $\sigma_t = s\sigma_{ci}/m_b$, see [3]. Next, one can see that the function g has the following structure for both the models:

$$g(\boldsymbol{\sigma}) = \hat{g}_1(\sigma_1) - \hat{g}_3(\sigma_3),$$

where $\hat{g}_1$ and $\hat{g}_3$ are increasing, convex and twice differentiable functions. By extending the results from [10], it is possible to show that such functions g are convex and they subdifferentials satisfy

$$\begin{aligned} \partial g(\boldsymbol{\sigma}) = \Big\{ \boldsymbol{\nu} = \sum_{i=1}^{3} \nu_i \mathbf{e}_i \otimes \mathbf{e}_i \;\Big|\; & (\mathbf{e}_1, \mathbf{e}_2, \mathbf{e}_3) \in V(\boldsymbol{\sigma}); \\ & \hat{g}_1'(\sigma_1) \geq \nu_1 \geq \nu_2 \geq \nu_3 \geq -\hat{g}_3'(\sigma_3);\ \sum_{i=1}^{3} \nu_i = \hat{g}_1'(\sigma_1) - \hat{g}_3'(\sigma_3); \\ & (\nu_1 - \hat{g}_1'(\sigma_1))(\sigma_1 - \sigma_2) = 0;\ (\nu_3 + \hat{g}_3'(\sigma_3))(\sigma_2 - \sigma_3) = 0 \Big\}, \end{aligned}$$

where $\hat{g}_1'$, $\hat{g}_3'$ denote the derivatives of $\hat{g}_1$, $\hat{g}_3$ and

$$V(\boldsymbol{\sigma}) = \{(\mathbf{e}_1, \mathbf{e}_2, \mathbf{e}_3) \in [\mathbb{R}^3]^3 \mid \mathbf{e}_i \cdot \mathbf{e}_j = \delta_{ij};\ \boldsymbol{\sigma}\mathbf{e}_i = \sigma_i \mathbf{e}_i,\ i,j = 1,2,3;\ \sigma_1 \geq \sigma_2 \geq \sigma_3\}.$$

If $\sigma_1 > \sigma_2 > \sigma_3$ then $\nu_1 = \hat{g}_1'(\sigma_1)$, $\nu_2 = 0$, and $\nu_3 = -\hat{g}_3'(\sigma_3)$, and thus g is differentiable at $\boldsymbol{\sigma}$. Otherwise, g is not differentiable at $\boldsymbol{\sigma}$ and ν_1, ν_2, ν_3 are not uniquely defined.

Let us recall that the unknown stresses tensor $\boldsymbol{\sigma} := \boldsymbol{\sigma}_k$ satisfies $f(\boldsymbol{\sigma}) = 0$ if the plastic correction (the return mapping) occurs. In such a case, $\boldsymbol{\sigma}$ lies on the

surface of the Mohr-Coulomb or Hoek-Brown pyramid. With respect to the ordering $\sigma_1 \geq \sigma_2 \geq \sigma_3$, we split the pyramidal surface into four parts: smooth portion ($\sigma_1 > \sigma_2 > \sigma_3$), the left (curved) edge ($\sigma_1 = \sigma_2 > \sigma_3$), the right (curved) edge ($\sigma_1 > \sigma_2 = \sigma_3$), and the apex ($\sigma_1 = \sigma_2 = \sigma_3 = \sigma_t$). This terminology was introduced in [4]. For each of these cases, one can specify the set $\partial g(\boldsymbol{\sigma})$ and consequently, the form of the return mapping. For example, if the return to the left edge occurs then $\hat{g}_1'(\sigma_1) \geq \nu_1 \geq \nu_2 \geq 0$, $\nu_1 + \nu_2 = \hat{g}_1'(\sigma_1)$, $\nu_3 = -\hat{g}_3'(\sigma_3)$ hold. These conditions are not usual in engineering practice but they can simplify the construction of the return mapping and help to find a correct return type.

In case of the elastic-perfectly plastic Mohr-Coulomb model, one can find decision criteria for each return type and even derive a close form of the constitutive operator $\boldsymbol{T}$, see e.g. [4, 10]. However, the function $\boldsymbol{T}$ is only in an implicit form for the Hoek-Brown model. In [3], the following return-mapping scheme was proposed. First, the return to the apex is tested. In this case, the solution must satisfy $\sigma_1 = \sigma_2 = \sigma_3 = \sigma_t$ and it is possible to derive necessary and sufficient conditions for this return type. If the return to the apex does not occur, the return to the smooth portion of the yield surface is tested and the corresponding problem has to be solved iteratively. After finding a solution candidate, we decide about its admissibility. If it is not admissible, one can decide using this candidate whether the return to the left or right curved edge occurs. We plan in our future work to complete this solution concept by rigorous analysis based on the subdifferential-based treatment and show that the operator $\boldsymbol{T}$ is well-defined.

In order to construct a generalized derivative of $\boldsymbol{T}$, we use the so-called eigenprojections and their derivatives, see [4]. For the sake of brevity, we introduce it only for a tensor $\boldsymbol{\varepsilon}^{tr}$ with three different eigenvalues $\varepsilon_1^{tr} > \varepsilon_2^{tr} > \varepsilon_3^{tr}$. Then, the spectral decomposition of $\boldsymbol{\varepsilon}^{tr}$ satisfies

$$\boldsymbol{\varepsilon}^{tr} = \sum_{i=1}^{3} \varepsilon_i^{tr} \mathbf{e}_i^{tr} \otimes \mathbf{e}_i^{tr}, \quad \mathbf{e}_i^{tr} \otimes \mathbf{e}_i^{tr} = \boldsymbol{E}_i^{tr} = \frac{(\boldsymbol{\varepsilon}^{tr} - \varepsilon_j^{tr}\boldsymbol{I})(\boldsymbol{\varepsilon}^{tr} - \varepsilon_k^{tr}\boldsymbol{I})}{(\varepsilon_i^{tr} - \varepsilon_j^{tr})(\varepsilon_i^{tr} - \varepsilon_k^{tr})}, \quad i = 1, 2, 3.$$

We say that the second-order tensors $\boldsymbol{E}_1^{tr}$, $\boldsymbol{E}_2^{tr}$, and $\boldsymbol{E}_3^{tr}$ are the *eigenprojections* of $\boldsymbol{\varepsilon}^{tr}$. If we consider the eigenvalues as functions depending on $\boldsymbol{\varepsilon}^{tr}$, then their derivatives satisfy $D\varepsilon_i^{tr}(\boldsymbol{\varepsilon}^{tr}) = \boldsymbol{E}_i^{tr}$, $i = 1, 2, 3$. Next, the derivative of $\boldsymbol{E}_i^{tr}$ is the fourth-order tensor and can be found in the following form:

$$\begin{aligned} D\boldsymbol{E}_i^{tr}(\boldsymbol{\varepsilon}^{tr}) := \mathbb{E}_i^{tr} \quad = \quad & \frac{\mathrm{D}((\boldsymbol{\varepsilon}^{tr})^2) - (\varepsilon_j^{tr} + \varepsilon_k^{tr})\mathbb{I} - (2\varepsilon_i^{tr} - \varepsilon_j^{tr} - \varepsilon_k^{tr})\boldsymbol{E}_i^{tr} \otimes \boldsymbol{E}_i^{tr}}{(\varepsilon_i^{tr} - \varepsilon_j^{tr})(\varepsilon_i^{tr} - \varepsilon_k^{tr})} \\ & - \frac{(\varepsilon_j^{tr} - \varepsilon_k^{tr})[\boldsymbol{E}_j^{tr} \otimes \boldsymbol{E}_j^{tr} - \boldsymbol{E}_k^{tr} \otimes \boldsymbol{E}_k^{tr}]}{(\varepsilon_i^{tr} - \varepsilon_j^{tr})(\varepsilon_i^{tr} - \varepsilon_k^{tr})}, \end{aligned}$$

where $i \neq j \neq k \neq i$.

Setting $\boldsymbol{\varepsilon}^{tr} := \boldsymbol{\varepsilon}_k - \boldsymbol{\varepsilon}^p_{k-1} + t_k\boldsymbol{\varepsilon}_0/t_{\max}$ and assuming that $\varepsilon^{tr}_1 > \varepsilon^{tr}_2 > \varepsilon^{tr}_3$, one can specify the form of the constitutive function $\boldsymbol{T}$ and its generalized derivative [10]:

$$\boldsymbol{\sigma}_k = \boldsymbol{T}\left(\boldsymbol{\varepsilon}^{tr}\right) = \sum_{i=1}^{3} \sigma_i(\boldsymbol{\varepsilon}^{tr})\boldsymbol{E}^{tr}_i, \quad \mathrm{D}\boldsymbol{T}\left(\boldsymbol{\varepsilon}^{tr}\right) = \sum_{i=1}^{3} \left[\sigma_i(\boldsymbol{\varepsilon}^{tr})\mathbb{E}^{tr}_i + \boldsymbol{E}^{tr}_i \otimes \mathrm{D}\sigma_i(\boldsymbol{\varepsilon}^{tr})\right].$$

Here, $\sigma_1, \sigma_2, \sigma_3$ are eigenvalues of the unknown stress tensor $\boldsymbol{\sigma}_k$. They depends on $\boldsymbol{\varepsilon}^{tr}$. $\mathrm{D}\sigma_i$ denotes a generalized derivative of σ_i, $i = 1, 2, 3$. It is necessary to use the implicit function theorem to find these derivatives.

4. Numerical example

In this section, we compare the elastic and elastic-plastic approaches to the prediction of EDZ. The comparison is illustrated on a plane strain problem inspired by a case study of the TSX experiment performed in the depth about 500 meters in Underground Research Laboratory in Canada, see [8].

The geometry and the finite element mesh are depicted in Figure 2. In particular, it is considered an elliptic tunnel profile with the diameters 4.375 and 3.5 meters. The initial stress tensor $\boldsymbol{\sigma}_0$ is assumed to be constant in the whole domain and its non-zero components have the following sizes: $\sigma_{0,1} = -45$ MPa, $\sigma_{0,2} = -11$ MPa, and $\sigma_{0,3} = -60$ MPa. The largest principle stress $\sigma_{0,3}$ is aligned with the tunnel axis and it is included to the model through the Mohr-Coulomb plastic criterion. The remaining principle stresses are depicted in Figure 2. The excavation process took time 17 days. So we choose $t_{\max} = 17$ days and consider 17 time steps. Next, we set $E = 60$ GPa, $\nu = 0.2$, $c = 17$ MPa, $\phi = \psi = 26°$. The strength parameters c and ϕ were chosen much lower than in [8] in order to highlight the difference between the elastic and elastic-plastic approaches. We use P2 finite elements and 7-point quadrature on each triangular element. The problems were implemented within in-house codes in Matlab. Some of them are available for download, see [2], and their Python's counterparts can be downloaded from [11].

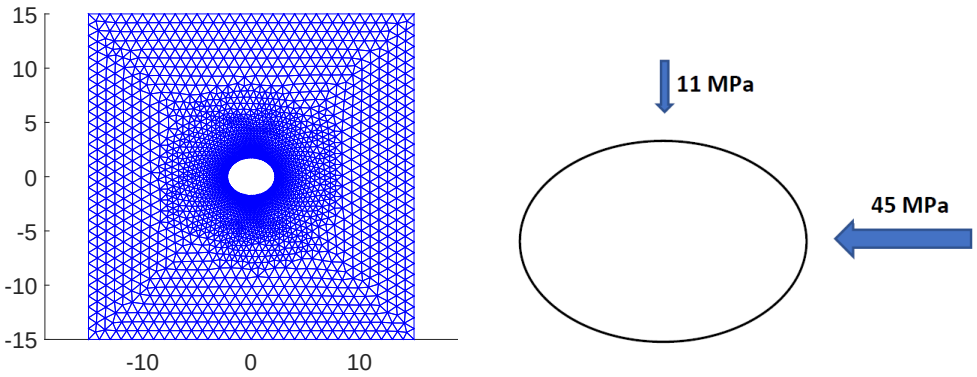

Figure 2: The geometry and the mesh for the plane strain problem. The sizes are in meters.

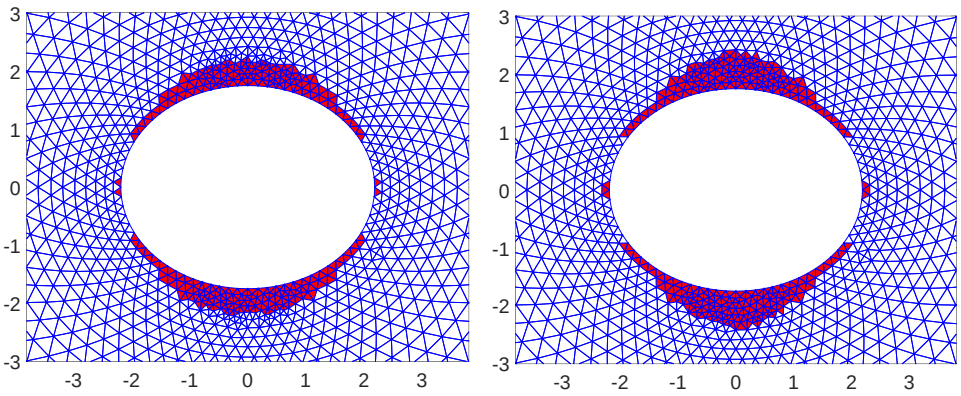

Figure 3: Comparison of failure zones for the elastic (left) and the elastic-plastic (right) models.

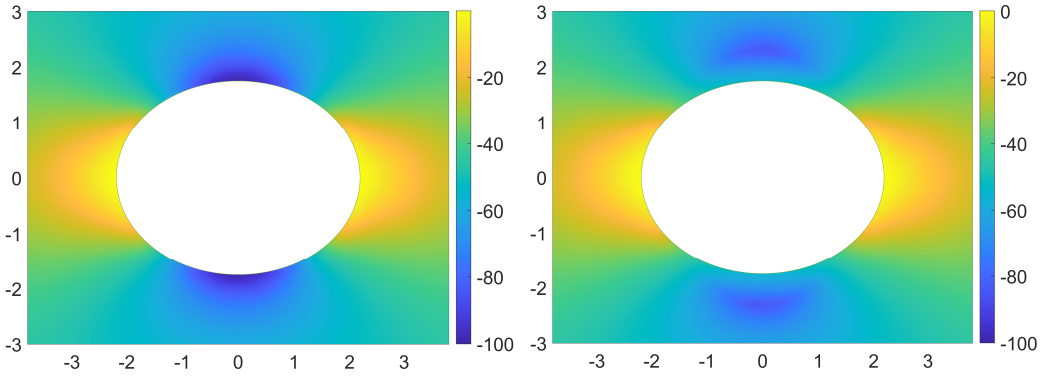

Figure 4: Comparison of horizontal stresses for the elastic (left) and the elastic-plastic (right) models. The scales are in MPa.

The comparison of failure zones computed for the elastic and elastic-plastic models are depicted in Figure 3. The zones for the elastic model are created by such elements where the Mohr-Coulomb criterion is not satisfied. They are rounded around the tunnel wall. In case of the elastic-plastic model, the zones represent elements with positive plastic multiplier. They have a typical V-notch shape that can be also observed within in-situ experiments.

In Figure 4, horizontal stresses are compared for the approaches. The elastic model admit higher stress concentrations (about 100 MPa) on the tunnel top and bottom unlike the elastic-plastic model where these concentrations are only about 50 MPa.

Figure 5 compares the total displacement and 300 times enlarged deformed shapes. For linear elasticity, we observe the contraction of the rock mass on the top and bottom of the tunnel. On the other hand, the dilatation is visible there in case of the elastic-plastic model. For better visualization of the contraction/dilatation, we compare vertical displacements on the tunnel top in Figure 6. We see that the plastic response is strongly nonlinear from the tenth time step leading to the dilatation.

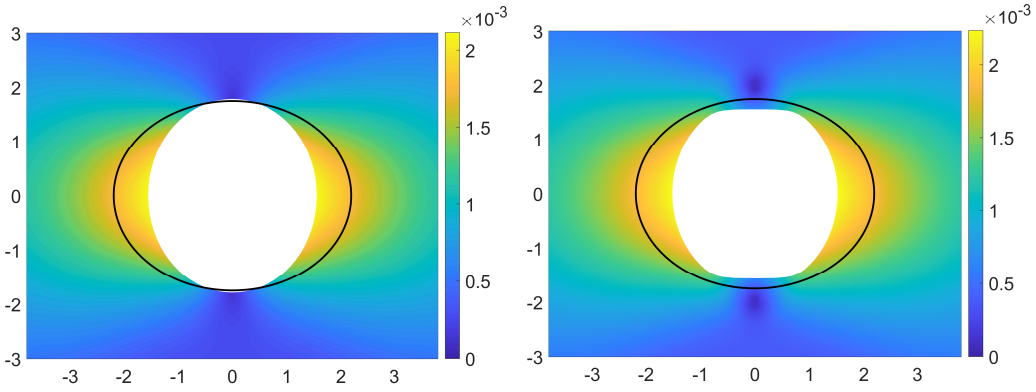

Figure 5: Comparison of total displacements and deformed shapes for the elastic (left) and the elastic-plastic (right) models. The scales are in meters.

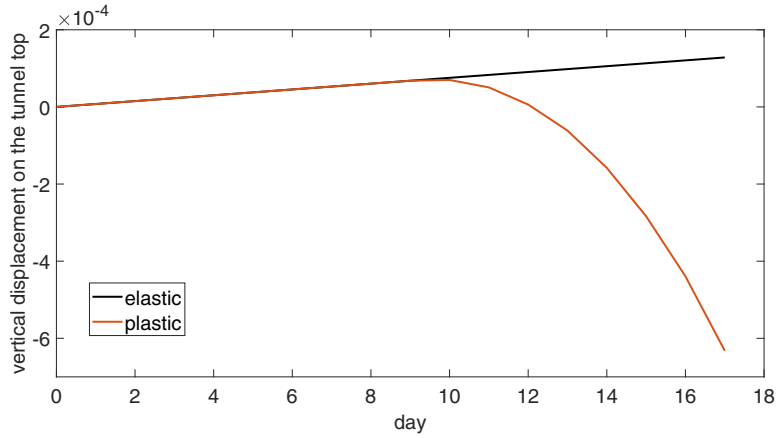

Figure 6: Evolution of the vertical displacements (in meters) on the tunnel top.

5. Conclusion

This contribution was a brief introduction to EDZ for deep tunnels in crystalline rocks. For prediction of EDZ, the elastic and elastic-plastic models were used. A scheme of numerical solution of the elastic-plastic problem was introduced. A particular interest was devoted to the Mohr-Coulomb and Hoek-Brown failure criteria. The subdifferential-based treatment to their constitutive solution was recommended. Finally, the elastic and elastic-plastic approaches to modeling of EDZ were compared on an illustrative numerical example.

Acknowledgements

This work was supported by grant No. TK02010118 of the Technology Agency of the Czech Republic.

References

[1] Andersson, J. C., Martin, C. D. and Stille, H.: The Äspö pillar stability experiment: part II—rock mass response to coupled excavation-induced and thermal-induced stresses. International Journal of Rock Mechanics and Mining Sciences **46**(5) (2009), 879–895.

[2] Čermák, M., Sysala, S. and Valdman, J.: Efficient and flexible MATLAB implementation of 2D and 3D elastoplastic problems. Applied Mathematics and Computation **355** (2019), 595–614.

[3] Clausen, J. and Damkilde, L.: An exact implementation of the Hoek–Brown criterion for elasto-plastic finite element calculations. International Journal of Rock Mechanics and Mining Sciences **45**(6) (2008), 831–847.

[4] de Souza Neto, E. A., Peric, D. and Owen, D. R.: *Computational methods for plasticity: theory and applications.* John Wiley & Sons, 2011.

[5] Hoek, E. and Brown, E. T.: The Hoek–Brown failure criterion and GSI–2018 edition. Journal of Rock Mechanics and Geotechnical Engineering **11**(3) (2019), 445–463.

[6] Hoek, E., Carranza-Torres, C. and Corkum, B.: Hoek-Brown failure criterion-2002 edition. In: *Proceedings of NARMS-Tac* **1**(1) (2002), 267–273.

[7] Perras, M. A. and Diederichs, M. S.: Predicting excavation damage zone depths in brittle rocks. Journal of Rock Mechanics and Geotechnical Engineering **8**(1) (2016), 60–74.

[8] Rutqvist, J., Börgesson, L., Chijimatsu, M., Hernelind, J., Jing, L., Kobayashi, A. and Nguyen, S.: Modeling of damage, permeability changes and pressure responses during excavation of the TSX tunnel in granitic rock at URL, Canada. Environmental Geology **57**(6) (2009), 1263–1274.

[9] Sysala, S., Cermak, M., Koudelka, T., Kruis, J., Zeman, J. and Blaheta, R.: Subdifferential-based implicit return-mapping operators in computational plasticity. ZAMM **96** (2016), 1318–1338.

[10] Sysala, S., Čermák, M. and Ligurský, T.: Subdifferential-based implicit return-mapping operators in Mohr-Coulomb plasticity. ZAMM **97** (2017), 1502–1523.

[11] https://github.com/MartinBeseda/FEM-ElastoPlasticity